Laser and Particle Beams (2007), *25*, 313–319. Printed in the USA.

DOI: 10.1017/S0263034607000171

Electron acceleration by high current-density relativistic electron bunch in plasmas

C.T. ZHOU,[1,2] M.Y. YU,[2,3] AND X.T. HE[1,2]

[1]Institute of Applied Physics and Computational Mathematics, Beijing, People's Republic of China
[2]Institute for Fusion Theory and Simulation, Zhejiang University, Hangzhou, People's Republic of China
[3]Institut für Theoretische Physik I, Ruhr-Universität Bochum, Bochum, Germany

(Received 7 January 2007; Accepted 10 February 2007)

Abstract

Electron acceleration by a short high-current relativistic electron bunch (EB) in plasmas at three characteristic densities is studied by particle-in-cell simulation. It is found that if the EB is appropriately matched to the background plasma, the blowout space-charge field of the EB can accelerate the trailing bunch electrons at very high energy gain rate. This high energy gain, as well as the large-amplitude wakefield, the turbulent small-scale electron plasma waves, and the formation of large current peaks, are studied. The evolution of the EB, its blowout field, and other related parameters are shown to be self-similar.

Keywords: Beam-plasma interaction; High-current particle accelerator; PIC simulation; Small-scale turbulent plasma waves

1. INTRODUCTION

Plasma wakefields can be generated using short intense pulses of laser light (Tajima & Dawson, 1979; Esarey *et al.*, 1997; Malka *et al.*, 2002; Niemann *et al.*, 2003; Geddes *et al.*, 2004; Faure *et al.*, 2004; Kawata *et al.*, 2005; Leemans *et al.*, 2006), electrons, or positrons (Lee *et al.*, 2000; Lotov, 2004; Hogan *et al.*, 2005; Lu *et al.*, 2005; Lifshitz *et al.*, 2006; Mellado *et al.*, 2006; Zhou *et al.*, 2006; Nakamura *et al.*, 2006). An intense ultrashort laser or particle pulse can excite large-amplitude relativistic wake plasma waves that can in turn accelerate the local plasma electrons to beyond 100 MeV. The accelerating gradient of the wakefield can be greater than 100 GeV/m, but the acceleration length is limited to about a millimeter. On the other hand, a tightly packed electron or positron bunch can also create a wakefield, and the energy gain by the accelerated electrons can reach a rate of several 100s of MeV/m, or even GeV/m, over 1 m.

Acceleration of electron and positron bunches in plasmas has been extensively investigated for more than a decade (Hora *et al.*, 2000*b*, 2002; Niemann *et al.*, 2003; Malka *et al.*, 2004; Mellado *et al.*, 2006; Neff *et al.*, 2006; Koyama *et al.*, 2006; Sakai *et al.*, 2006). Recently, there has been much interest in the acceleration of particles by plasma wakefields created by short and intense charged-beam pulses. It is well known from the linear theory that the wake amplitude optimum for acceleration is a function of the bunch length σ_z^{-2} (Lee *et al.*, 2000). For very narrow ($k_p\sigma_r \ll 1$, where $k_p = \omega_p/c \sim 1.88 \times 10^{-6} n_e^{1/2}\,\mathrm{cm}^{-1}$ is the inverse collisionless skin depth, and σ_r and σ_z are the bunch radius and length, respectively) bunches, the latter relation is modified by $\sigma_z^{-2} \cdot \ln(n_b^{-1/2}\,\sigma_r)$ (Lu *et al.*, 2005). The maximum wake amplitude scales with $N_b\,/\sigma_z^2$, where N_b is the number of bunch particles, and this scaling holds well into the nonlinear blowout regime. Recently, it was shown experimentally that a compressed and focused 28.5 GeV electron bunch (EB) with 1.8×10^{10} electrons can achieve an energy gain by 7% of the trailing brunch electrons at more than 27 GeV/m (Hogan *et al.*, 2005). Short relativistic EBs can thus be useful of wakefield acceleration of particles in future high-energy particle accelerators (Mourou *et al.*, 2006).

When a short highly charged relativistic EB propagates in a plasma, the blowout space-charge field can considerably decelerate the particles at the front part of the EB and accelerate that at its back. They can also excite intense coherent wake plasma oscillations, which in turn accelerate the background plasma electrons there. In the ultra-strong wave and

Address correspondence and reprint requests to: C. T. Zhou, Institute of Applied Physics and Computational Mathematics, PO Box 8009, Beijing 100088, People's Republic of China. E-mail: zcangtao@iapcm.ac.cn

space-charge electric fields, most of the driven electrons become highly relativistic. The background plasma density plays an important role in determining the evolution scenario of the bunch and plasma electrons. In particular, interactions involving high-density relativistic EB and plasma can be expected to be quite different from that of the well-studied interactions involving low or moderate EB and plasma densities. It is thus of interest to investigate the properties and energy-transfer efficiency in interactions involving high densities.

Although nonlinear theories for relativistic plasma wakefields in the blowout regime exist, particle-in-cell (PIC) simulation still remains the major tool for more realistic studies of the plasma response and the energy loss and gain by the plasma and bunch particle. In this paper, we use PIC simulation to investigate the dynamics of the relativistic particles, local electron accumulation, and heating, as well as how the overall energy gain by the bunch electrons can be maximized. Three characteristic cases, corresponding to underdense, critical density, and over dense plasmas (with respect to the high-density EB), shall be considered and compared. It is shown that the energy gain (or loss) by the bunch electrons is linearly proportional to the propagation distance. The ratio of the number of bunch electrons that gain energy to the total number of bunch electrons remains practically constant. In the critical-density case, a 20 μm 28.5 GeV EB can result in energy gain by ~45% of the bunch electrons, and some of the latter can achieve gain of over 80 GeV/m under available experimental conditions. The high energy-conversion efficiency is a result of appropriate matching of the bunch and plasma parameters, such that a large number of bunch electrons can be accelerated by a strong electric field.

2. CONFIGURATION AND PARAMETERS

We start with a brief description of the simulation configuration and approach. We shall assume that the high-current EB propagates in a preformed cylindrically symmetric channel of lithium plasma. For treating the present problem, standard PIC codes (Birdsall & Langdon, 1985) would normally need a large number of simulation cells and very small time steps because of, for example, the limitation imposed by Debye-length instability, and instability of the electromagnetic solvers at long running times. An implicit particle push based on the algorithm of Hewett and Langdon (1987), as well as an implicit electromagnetic solver, are thus employed. We have also modified the standard PIC algorithm to include an energy conserving scheme (Lipatov, 2002; Zhou *et al.*, 2006; Zhou & He, 2007) that removes the Debye-length instability. Because of the implicit energy-conserving algorithms, the spatial cell size is permitted to be large compared to both the skin depth and Debye length. The code is thus constrained only by the time- and space-step sizes, and should be suitable for direct simulation of large-scale and high-density beam-plasma interactions.

The simulation box (r, z) is 0.02 cm × 0.1 cm. The mesh resolution is 1000 × 5000 cells, with 16 plasma particles, and up to four injected bunch particles in each cell. The temporal resolution is $\delta t = 2$ fs. We also include an initial transverse bunch-electron temperature $kT_b = 1$ MeV. The background plasma is fully ionized lithium vapor. The initial temperature for plasma electrons and ions is 125 eV (since the ionization potential for the first, second, and third electrons are 5.4 eV, 75.6 eV, 122.5 eV, respectively).

The EB has a bi-Gaussian density profile given by $n_b(r,\ \xi) = N_b \exp[-r^2/2\sigma_r^2 - \xi^2/2\sigma_z^2]$, where $\xi = z - v_b t$, $v_b \sim c$, $N_b = 2 \times 10^{10}$, $\sigma_r = 10$ μm, and $\sigma_z = 20$ μm. The average bunch density is thus $n_b = N_b/(2\pi)^{3/2}\ \sigma_z\ \sigma_r^2 \sim 6.3 \times 10^{17}\ \mathrm{cm}^{-3}$ and the EB current density is $J_b \sim -2.7 \times 10^9\ \mathrm{A/cm}^2$, corresponding to a current of $I \sim 8.6$ KA. We note that the latter is much larger than that of the more moderate-density ($n_b \lesssim 10^{15}\ \mathrm{cm}^{-3}$) EBs considered earlier (Lee *et al.*, 2000; Zhou *et al.*, 2006). The induced space-charge field is $E_z^{\mathrm{acc}} \sim r_e\ N_b\ k_p\ E_0 \sim 10^{-8}\ (n_b n_e)^{1/2}\ \mathrm{V/cm}$, where $E_0 = mc\omega_p/e \sim 0.96\ n_e^{1/2}\ \mathrm{V/cm}$ is the classical wave-breaking field, $n_e[\mathrm{cm}^{-3}]$ is the plasma density, $r_e = e^2/mc^2 \sim 2.82 \times 10^{-13}$ cm is the classical electron radius, $\omega_p = (4\pi\ n_e\ e^2/m_e)^{1/2}$ is the plasma frequency of the background plasma, and c, m, and e are the speed of light in a vacuum, electron rest mass, and charge, respectively (Esarey *et al.*, 1997). The inverse skin depth can then be expressed as $k_p = \omega_p/c \sim 1.88 \times 10^{-6}\ n_e^{1/2}\ \mathrm{cm}^{-1}$. Thus, if $n_b \sim n_e \sim 10^{18}\ \mathrm{cm}^{-3}$, it should be possible to have E_z^{acc} greater than 100 GV/m. In other words, energy gain at ~100 GeV/m can be realized if the bunch and plasma parameters are appropriately matched.

3. WAKEFIELD AND ELECTRON ACCELERATION

The simulation results are summarized in Figure 1 for three characteristic cases, corresponding to the plasma densities: (1) $n_e[\mathrm{cm}^{-3}] = 3 \times 10^{16}$ (left column, underdense plasma, and corresponding to classical acceleration of plasma electrons in the downstream wakefield), (2) 1.5×10^{18} (center column, EB and plasma densities of the same order, corresponding to strong acceleration of bunch, and plasma electrons), and (3) 3×10^{18} (right column, dense plasma, corresponding to weaker acceleration of bunch, and wake electrons but strong plasma heating). The rows show the corresponding spatial distribution, the relativistic factor γ, or the energy or momentum associated with electron motion along z normalized by mc^2 or mc, respectively, and the temperature of the bunch and plasma electrons.

Case 1, where $n_b \gg n_e = 3 \times 10^{16}\ \mathrm{cm}^{-3}$ represents the classical downstream acceleration of electrons in an underdense plasma by the wakefield of an EB. As shown in Figure 1d, the plasma electrons can be accelerated to energies up to $\gamma \sim 60$, and the energized electrons are highly localized in the compression regions of the wake. Figure 1g shows that there is a strong enhancement of the local electron

https://doi.org/10.1017/S0263034607000171 Published online by Cambridge University Press

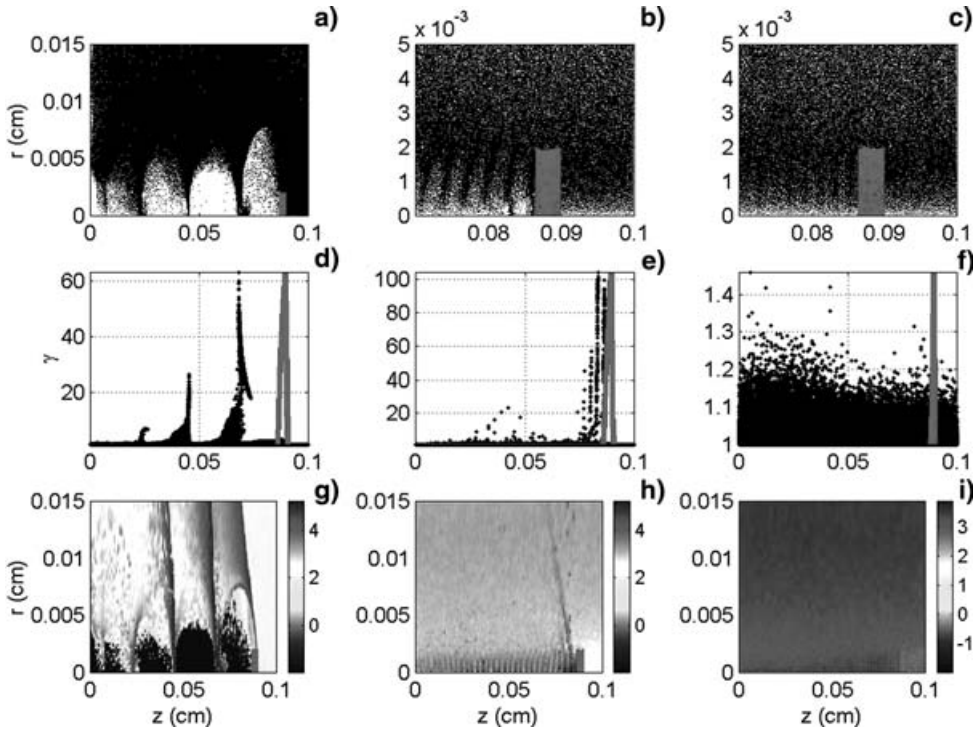

Fig. 1. The behavior of the background (channel) plasma and EB electrons at $t = 3$ ps. The EB consists of 28.5 GeV electrons with $\sigma_r = 10$ μm, $\sigma_z = 20$ μm, and average density $\sim 6.3 \times 10^{17}$ cm^{-3}. The first row shows the spatial distributions of the channel electrons (tiny black dots). The channel contains lithium plasma with densities n_e [cm^{-3}] $= 3 \times 10^{16}$ (**a**), 1.5×10^{18} (**b**), and 3×10^{18} (**c**), respectively. The subfigures (**d**) – (**f**) show the corresponding normalized momentum (or energy) $\gamma = P_z/m_e c$ of the plasma electrons along the propagation direction, and (**g**) – (**h**) show the corresponding plasma-electron temperature, respectively. The EB is shown different color, and the EB density profile given in (d) – (f) is in arbitrary units. Note that the axes scales in (b) and (c) are enlarged.

temperature in the compression regions that are also radially extended. Thus, the energized plasma electrons are spatially separated from the EB, which remains nearly unchanged.

In terms of the energy-transfer efficiency, it is desirable to have most of the acceleration by the initial space-charge field directly. This can be achieved by tailoring the EB profile and/or increasing n_e. By trying different n_e values, we found that Case 2, where $n_b \lesssim n_e$, that is, the plasma is at an effective critical density, gives a good solution to the problem, and this case is of our main interest. Figure 1b shows a trailing wakefield of much less longitudinal extent as well as wavelength. It is also radially localized to $r \sim \sigma_r$, i.e., comparable to that of the EB. Furthermore, in Figure 1e, there is only one peak of highly energized (with $\gamma \sim 100$) electrons, and it partially overlaps the EB. The electrons in the second half of the bunch as well as in the adjacent background plasma are accelerated by the original blowout field. We emphasize that, an important property of this case is that the characteristic dimensions of the blowout region, as well as the downstream wake, are on the order of the EB. Figure 1h also shows that strong increase of the plasma temperature is again localized in the regions with energized electrons.

Further increase of n_e leads to reduced acceleration, as can be seen in Figures 1c and 1f for Case 3, where $n_b \sim 0.2 n_e$. Only a weak and rather incoherent short-wavelength wakefield is formed, together with little relativistic electron generation. Figures 1c, 1f, and 1i also show that the background plasma electrons are almost uniformly heated by the clearly visible widespread short-wavelength plasma wave turbulence. For a well-defined blowout region to exist in this low bunch density case, a more heavily charged EB is needed to displace the dense background electrons.

Next, we consider the acceleration of the bunch electrons. Figure 2 shows the radially averaged (over $0 \leq r \leq \sigma_r$) (a) longitudinal electric field $\langle E_z \rangle$, (b) radial electric field $\langle E_r \rangle$, (c) azimuthal magnetic field $\langle B_\theta \rangle$, and (d) current density $\langle J_z \rangle$. The corresponding profiles in the absence of the background plasma are given by the dashed curves. The EB density profile is schematically represented by the thick black curve (with the arrow indicating its propagation direction) in Figure 2a. In the absence of the background plasma, we see in Figures 2b and 2c, that the EB is associated with strong $\langle E_r \rangle$ and $\langle B_\theta \rangle$, but $\langle E_z \rangle$ is weak and axially extended. The strong $\langle E_r \rangle$ and $\langle B_\theta \rangle$ can easily induce additional relativistic electron motion. However, as the figures shows, these fields are significant only behind the EB. Nevertheless, they can act on the background plasma electrons. Accordingly, for Case 1, where the background plasma is underdense, the initial longitudinal space-charge field extends far downstream of the EB, and thus results in an extended wakefield of long wavelength in the plasma.

https://doi.org/10.1017/S0263034607000171 Published online by Cambridge University Press

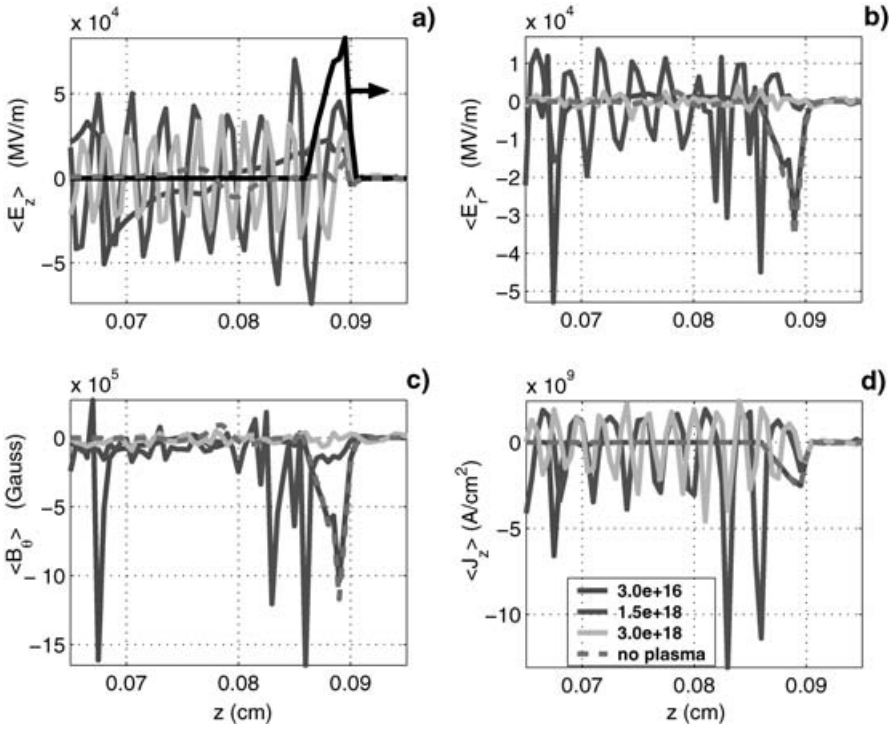

Fig. 2. Plasma waves excited by the EB (black curve in (a)). Radially averaged (*a*) longitudinal electric field $\langle E_z \rangle$, (*b*) radial electric field $\langle E_r \rangle$, (*c*) azimuthal magnetic field $\langle B_\theta \rangle$, and (*d*) current density $\langle J_z \rangle$. The insert in (d) identifies the Cases 1 to 3.

Although the plasma electrons are efficiently accelerated by the downstream wakefield, the bunch electrons can only lose energy. However, in Case 2, where n_e is optimized, Figure 2a shows that the EB overlaps the blowout region. Here, the blowout region spans one complete cycle of the space-charge field. As a result, the front part of the EB loses energy by expelling the plasma electrons, but the electrons in the trailing part of the EB are accelerated by the resulting space-charge field. In fact, here the strong transverse fields $\langle E_r \rangle$ and $\langle B_\theta \rangle$ at the back of the EB reinforce the action of the longitudinal space-charge field in energizing and returning the plasma electrons. For still higher plasma densities, such as those in Case 3, Figures 1c and 2a shows that there is very weak plasma electron blowout, and the EB is longer than one complete period of the original space-charge field. In this case, a part of the accelerated bunch electrons are decelerated, leading to reduced energy gain.

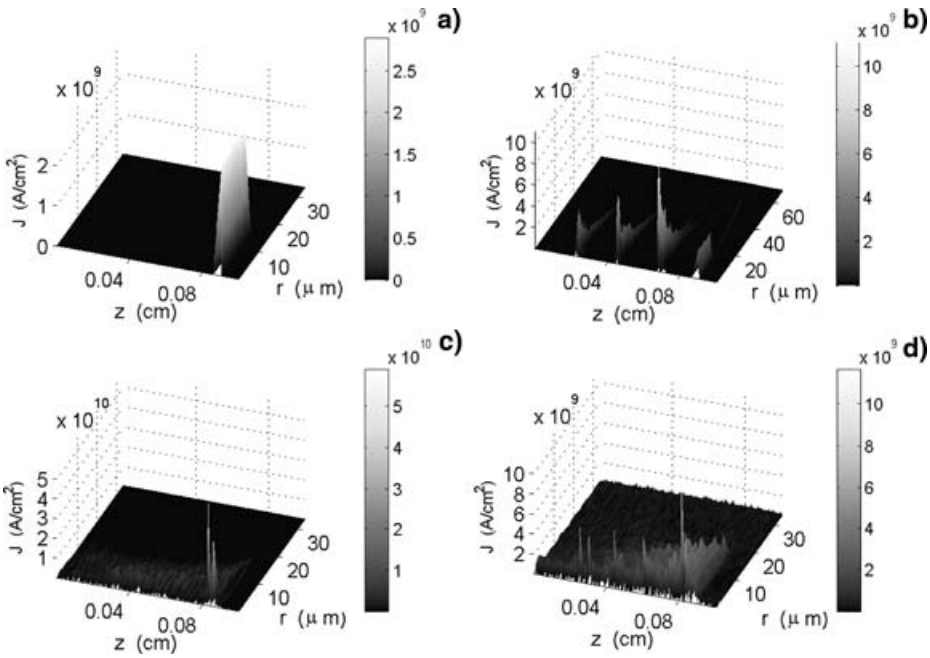

Fig. 3. The behavior of the *total* current density $J = \sqrt{J_r^2 + J_\theta^2 + J_z^2}$ for different background plasma densities. (**a**) no plasma, (**b**) Case 1, (**c**) Case 2, and (**d**) Case 3. Note that the intensity scale and color code in (c) are different from the others.

https://doi.org/10.1017/S0263034607000171 Published online by Cambridge University Press

Figure 2d shows the radially averaged current density. Without the plasma, the EB current density reaches -2.65×10^9 A/cm^2, which is in good agreement with the estimate above. When a background plasma is present, for Case 1, the plasma current density in the downstream wakefield can reach -6.6×10^9 A/cm^2, i.e., twice larger than that of the bunch alone. As expected, this peak is associated with that of $\langle E_r \rangle$ and $\langle B_\theta \rangle$ shown in Figures 2b and 2c, as well as the returning high-energy electrons in Figure 1d. It should also be noted that $\langle E_r \rangle$ and $\langle B_\theta \rangle$ for Case 3 are small, and is consistent with the small number of expelled, and therefore also the energetic returned, plasma electrons.

In order to visualize the overall, especially the radial, behavior of the EB, as well as its wake in the background plasma, we show in Figure 3 the spatial distribution of the total current density at $t = 3$ ps. Without the plasma, Figure 3a shows that the EB current density remains Gaussian, with very little dispersion. For Case 1, with underdense background plasma, Figure 3b (note the different radial scaling) shows three strong current peaks corresponding to the wake plasma oscillations behind the (relatively small) EB current peak, which is itself almost unchanged by the presence of the plasma. The wake current peaks also have considerable radial spread. For Case 2, with optimum electron acceleration, Figure 3c shows that the EB is represented by two large current peaks at the back of the EB, followed by weaker and somewhat incoherent wake oscillations. Comparing the magnitude of the front peaks with that of J_z corresponding to Case 2 in Figure 2d, we see that the perpendicular component is larger than the longitudinal one, indicating that much of the energy of the electrons returned by the initial space-charge field resides in their perpendicular velocities, although the peaks also correspond to maximum longitudinal acceleration. Besides the large-amplitude wakefield plasma wave, an EB can also excite incoherent small-scale electron plasma waves, as can be seen in Figure 3c. For case 3, with still larger n_e, one can clearly observe in Figure 3d, wide-spread small-scale plasma-wave turbulence. The large peaks at the EB as well as in the wakefield oscillations still exist. Turbulence can also be found far ahead of the EB, since it is composed of short-wavelength plasma waves at relativistic speeds. The turbulence efficiently and uniformly heats the background plasma, as can also be seen in Figures 1c and 1d for the temperature distribution.

It is of interest to look at the ratio $\mathcal{R} = \langle E_z \rangle^- / \langle E_z \rangle^+$, where the $-$ and $+$ signs denote the minimum and maximum of the longitudinal electric field. For the three cases considered here, one finds $\mathcal{R} \sim [51/23,74/45,35/27] \sim [2.2,1.6,1.3]$, respectively. We see that $\mathcal{R}$ is largest for Case 1. Although in this case, the plasma electrons are strongly accelerated in the downstream wake, the bunch electrons gain no net energy since the effective part of the space-charge field is behind the EB. For Case 2, despite a smaller $\mathcal{R}$, the plasma electrons as well as the trailing electrons in the EB are efficiently accelerated. The longitudinal space-charge as well as the trailing wake electric fields in the three cases are of similar magnitude (Figure 2a). The large difference in their effects lies in their structure and location, as well as the corresponding transverse fields, and how they act on the plasma and bunch electrons.

4. ENERGY GAIN AND LINEAR SCALING

We now consider the maximum and minimum energy gain or loss by the bunch electrons in the three cases. The EB energy is given by $\epsilon_{\rm EB} = (\gamma - 1)mc^2$. Figure 4 shows the envelopes of the highest and lowest values of the change $\Delta\epsilon_{\rm EB}$ in the energy of the electrons, as the EB propagates in plasmas of cases 1 to 3. The upper inset shows a series of snapshots of $\epsilon_{\rm EB}$ as the EB propagates in a Case 2 plasma. The enlarged profile on its right represents a snapshot of the bunch energy at 0.1 cm. As is well known, the leading electrons lose energy and the trailing ones gain energy. We also see that as the EB is compressed during the propagation, there is considerable energy spread. Except for Case 1, for which the EB does not gain energy at all, both the maximum energy gain and loss by the bunch electrons increases as the EB propagates, with the former considerably faster. The envelopes of the maximum and minimum bunch-electron energy are straight lines for all three cases, as well as under other physical and simulation conditions within the parameter range studied. This behavior can be roughly attributed to the fact that the blowout space-charge field and the EB are spatially and temporally concurrent as a self-organized system. However, the physical details of the system still need to be more quantitatively investigated.

As the EB is compressed in a self-similar manner (after the very initial deformation), the blowout field changes in the same way. For the same reason, the ratio $\mathcal{R}$ (in percent) of the number of energy-gaining bunch electrons to the total number of bunch electrons remains constant (see the center inset in Fig. 4). The numbers in the bottom inset gives the rates (in GeV/m) of the energy change $\Delta\epsilon_{\rm EB}$, with respect to the initial bunch-electron energy of 28.5 GeV. We see that about 45% of the bunch electrons gain energy in Case 2, and somewhat more than 35% in Case 3. As expected, in Case 1, all of the electrons in the EB lose energy. However, the corresponding wake plasma oscillations periodically accelerate the downstream plasma electrons to relativistic energies. Case 2 yields the maximum energy gain by the trailing bunch electrons (as well as loss by the leading bunch electrons). The highest energy gain can reach 82 GeV/m, and the number of electrons with energy greater than the original 28.5 GeV is $\sim 9 \times 10^9$. However, in this case, there is only weak acceleration of the downstream plasma electrons in the trailing wake oscillations. It is also of interest to note that in Case 3 of high background plasma density, for which the background plasma becomes rapidly turbulent, and there is no generation of high energy plasma electrons, the EB can still have $\sim 7 \times 10^9$ electrons with energy gain of up to 38 GeV/m.

https://doi.org/10.1017/S0263034607000171 Published online by Cambridge University Press

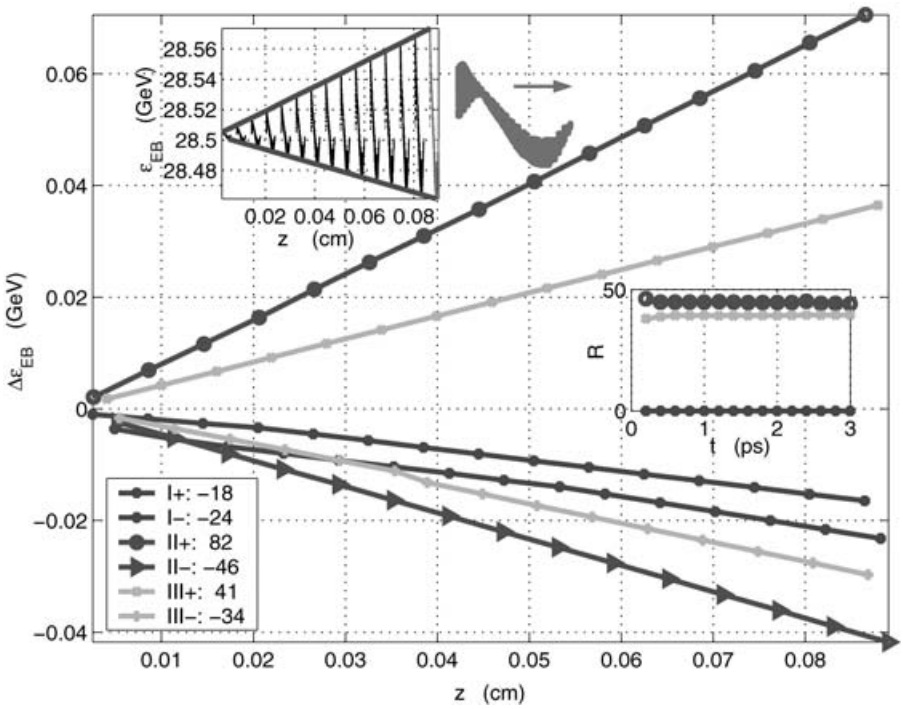

Fig. 4. Envelopes of the highest and lowest energy gain and loss by the bunch electrons as the EB propagates in plasmas of Cases 1 to 3. The legend for the curves is in the bottom inset. The upper inset shows snapshots of the ϵ_{EB} profile for Case 2. The enlarged profile on the right is a stretched snapshot at 0.1 cm. The center inset shows the percentage R of electrons accelerated to energies higher than the initial energy 28.5 GeV. The numbers in the bottom inset indicate the gradients (in GeV/m) of the envelopes of the maxima and minima of the bunch electron energy for Cases 1 to 3, and the plus and minus signs denote maximum and minimum gain (or loss), respectively.

5. SUMMARY

In summary, we have used two-dimensional PIC simulation to consider the acceleration of electrons to ultrahigh energies, when a dense short-pulse relativistic EB propagates in a plasma. The EB together with the blowout field, and therefore, all of the bunch-electron properties, evolve in a self-similar manner for underdense, critical, as well as overdense plasmas. In the near-optimum Case 2, about 45% of the bunch electrons gains energy and the gain can reach 82 GeV/m. When the background plasma density n_e is sufficiently large, turbulence of spatially widespread fast short-wavelength plasma waves can rapidly heat the entire plasma.

Since the simulation is two-dimensional, certain intrinsic higher dimensional effects such as the transverse hosing instability (Whittum *et al.*, 1992) of the EB has been precluded. However, the latter is not expected to be significant here since the background plasma is preformed and the EB as well as the time scale of interest are short. In applications where the background plasma is self-ionized by the EB or when much longer-distance propagation of the EB is needed, the hosing and other nonlinear instabilities (Hora, 2000*a*; Liu *et al.*, 2006) may occur and a three-dimensional and/or longer-time simulation would be needed. The results here should nevertheless be useful for estimating the EB energy gain and as a guide for a more analytical understanding of EB-plasma interaction at high energies and densities. They should also be useful for implementing new schemes of particle acceleration (Kawata *et al.*, 2005; Koyama *et al.*, 2006; Lifshitz *et al.*, 2006; Mangels *et al.*, 2006; Mellado *et al.*, 2006; Nakamura *et al.*, 2006; Sakai *et al.*, 2006) by intense lasers and EBs for various applications.

ACKNOWLEDGMENTS

This work is supported by the National Natural Science Foundation of China, Grant Nos. 10575013, 10576007, and 10335020, and the National High-Tech ICF Committee in China.

REFERENCES

Birdsall, C.K. & Langdon, A.B. (1985). *Plasma Physics via Computer Simulation*. New York: McGraw-Hill.

Esarey, E., Sprangle, P., Krall, J. & Ting, A. (1996). Overview of plasma-based accelerator concepts. *IEEE Trans. Plasma. Sci.* **24**, 252–288.

Esarey, E., Sprangle, P., Krall, J. & Ting, A. (1997). Self-focusing and guiding of short laser pulses in ionizing gases and plasmas. *IEEE J. Quan. Electron.* **33**, 1879–1914.

Faure, J., Glinec, Y., Pukhov, A., Kiselev, S., Gordienko, S., Lefebvre, E., Rousseau, J.-P., Burgy, F. & Malka, V. (2004). A laser-plasma accelerator producing monoenergetic electron beams. *Nature* **431**, 541–544.

Geddes, C.G.R., Toth, C.S., Tilborg, J., van Esarey, E., Schroeder, C.B., Bruhwiler, D., Nieter, C., Cary, J. & Leemans, W.P. (2004). High-quality electron beams from a laser wakefield accelerator using plasma-channel guiding. *Nature* **431**, 538–541.

Hewett, D.W. & Langdon, A.B. (1987). Electromagnetic direct implicit plasma simulation. *J. Comp. Phys.* **72**, 121–155.

Hogan, M.J., Barnes, C.D., Clayton, C.E., Decker, F.J., Deng, S., Emma, P., Huang, C., Iverson, R.H., Johnson, D.K., Joshi, C., Katsouleas, T., Krejcik, P., Lu, W., Marsh, K.A., Mori, W.B., Muggli, P., O'Connell, E., Oz, E., Siemann, R.H. & Walz, D. (2005). Multi-GeV Energy Gain in a Plasma-Wakefield Accelerator. *Phys. Rev. Lett.* **95**, 054802.

https://doi.org/10.1017/S0263034607000171 Published online by Cambridge University Press

Hora, H. (2000*a*). *Laser Plasma Physics: Forces and the Nonlinearity Principle*. Bellingham, WA: Spie Press.

Hora, H., Hoelss, M., Scheid, W., Wang, J.X., Ho, Y.K., Osman, F. & Castillo, R. (2000*b*). Principle of high accuracy of the nonlinear theory for electron acceleration in vacuum by lasers at relativistic intensities. *Laser Part. Beams* **18**, 135–144, and the references therein.

Hora, H., Osman, F., Castillo, R., Collins, M., Stait-Gardener, T., Chan, W.K., Hölss, M., Scheid, W., Wang, J.J. & Ho, Y.K. (2002). Laser-generated pair production and Hawking-Unruh radiation. *Laser Part. Beams* **20**, 79–86.

Kawata, S., Kong, Q., Miyazaki, S., Miyauchi, K., Sonobe, R., Sakai, K., Nakashima, K., Masuda, S., Ho, Y.K., Miyanakga, N., Limpouch, J. & Andreev, A.A. (2005). Electron bnch acceleration and trapping by ponderomotive force of intense short-pulse laser. *Laser Part. Beams* **23**, 61–68.

Koyama, K., Adachi, M., Miura, E., Kato, S., Masuda, S., Watanabe, T., Ogata, A. & Tanimoto, M. (2006). Monoenergetic electron beam generation from a laser-plasma accelerator. *Laser Part. Beams* **24**, 95–100.

Lee, S., Katsouleas, T., Hemker, R. & Mori, W.B. (2000). Simulations of a meter-long plasma wakefield accelerator. *Phys. Rev. E* **61**, 7014–7021.

Leemans, W.P., Nagler, B., Gonsalves, A.J., Toth, C., Nakamura, K., Geddes, C.G.R., Esarey, E., Schroeder, C.B. & Hooker, S.M. (2006). GeV electron beams froma centimetre-scale accelerator. *Nature Physics* **2**, 696–699.

Lifshitz, A.F., Faure, J., Glinec, Y., Malka, V. & Mora, P. (2006). Proposed scheme for compact GeV laser plasma accelerator. *Laser Part. Beams* **24**, 255–260.

Lipatov, A.S. (2002). *The Hybrid Multiscale Simulation Technology*. Berlin: Springer.

Lotov, K.V. (2004). Blowout regimes of plasma wakefield acceleration. *Phys. Rev. E.* **69**, 046405.

Liu, Z.J., Zhu, S.P., Cao, L.H., Zheng, C.Y. & Li, B. (2006). Self-organization of plasma due to electron beam instability. *Phys. Plasmas* **13**, 053103.

Lu, W., Huang, C., Zhou, M.M., Mori, W.B. & Katsouleas, T. (2005). Limits of linear plasma wakefield theory for electron or positron beams. *Phys. Plasmas* **12**, 063101.

Malka, V., Fritzler, S., Lefebvre, E., Aleonard, M.-M., Burgy, F., Chambaret, J.-P., Chemin, J.-F., Krushelnick, K., Malka, G., Mangles, S.P.D., Najmudin, Z., Pittman, M., Rousseau, J.-P., Scheurer, J.-N., Walton, B. & Dangor, A.E. (2002). Electron acceleration by a wake field forced by an intense ultrashort laser pulse. *Science*. **298**, 1596–1600.

Malka, V. & Fritzler, S. (2004). Electron and proton beams produced by ultra short laser pulses in the relativistic regime. *Laser Part. Beams* **22**, 399–405.

Mangels, S.P.D., Wlaton, B.R., Najmudim, Z., Dangor, A.E., Kruschelnik, K., Malka, V., Mangloskki, M., Lopes, N., Caras, C., Mendes, G. & Dorchies, F. (2006). Table-top laser-plasma accelerator as an electron radiographic sources. *Laser Part. Beams* **24**, 185–190.

Mellado, V.H., Hacyan, S. & Jauregui, R. (2006). Trapping and acceleration of charged particle in Bessel beams. *Laser Part. Beams* **24**, 559–566.

Mourou, G.A., Tajima, T. & Bulanov, S.V. (2006). Optics in the relativistic regime. *Rev. Mod. Phys.* **78**, 309–371.

Nakamura, T., Sakagami, H., Johzaki, T., Nakatomo, H. & Mima, K. (2006). Generation and transport of fast electrons inside cone targets irradiated by intense laser pulses. *Laser Part. Beams* **24**, 5–8.

Neff, S., Knobloch, R., Hoffmann, D.H.H., Tauschwitz, A. & Yu, S.S. (2006). Transport of heavy-ion beams in a 1 m free-standing plasma channel. *Laser Part. Beams* **24**, 71–80.

Niemann, C., Penache, D., Tauschwitz, A., Rosmej, F.B., Neff, S., Birkner, R., Constantin, C., Knobloch, R., Presura, R., Yu, S.S., Sharp, W.M., Ponce, D.M. & Hoffmann, D.H.H. (2003). Diagnostics of discharge channels for neutralized chamber transport in heavy ion fusion. *Laser Part. Beams* **21**, 13–15.

Sakai, K., Miyazaki, S., Kawata, S., Hasumi, S. & Kikuchi, T. (2006). High-energy-density attosecond electron beam production by intense short-pulse laser with a plasma separator. *Laser Part. Beams* **24**, 321–328.

Tajima, T. & Dawson, J.M. (1979). Laser electron accelerator. *Phys. Rev. Lett.* **43**, 267–270.

Whittum, D.H., Sharp, W., Yu, S.S., Lampe, M. & Joyce, G. (1992). Electron-hose instability in the ion-focused regime. *Phys. Rev. Lett.* **67**, 991–994.

Zhou, C.T., He, X.T. & Yu, M.Y. (2006). A comparison of ultrarelativistic electron- and positron-bunch propagation in plasmas. *Phys. Plasmas* **13**, 092109.

Zhou, C.T. & He, X.T. (2007). Influence of a large oblique incident angle on energetic protons accelerated from solid density plasmas by ultraintense laser pulses. *Appl. Phys. Lett.* **90**, 031503.